Supplementing Thermal Sunyaev-Zeldovich Effect Surveys with CCAT High-Angular-Resolution Follow-Up

Overview

We propose a program using the 25-m Cornell-Caltech Atacama Telescope (CCAT) to do high-angular-resolution thermal Sunyaev-Zeldovich (tSZ) effect follow-up observations of clusters detected in wide-area blind tSZ surveys. Such follow-up data on a subset of clusters will enable tests and calibration of the relation between tSZ flux and cluster mass and will help characterize these surveys' mass selection functions. These tests will ensure that these surveys have the best possible opportunity to derive precise constraints on the Dark Energy parameters Ω_Λ and w. This work will primarily use the prospective CCAT 150 GHz facility camera.

Personnel and Institutions Involved

The Cornell-Caltech Atacama Telescope is a prospective general-use 25-m submillimeter and mm-wave telescope currently under study by a large consortium of institutions, led by Cornell University, the California Institute of Technology, and NASA's Jet Propulsion Laboratory. The lead personnel on the study are

Study Lead: Riccardo Giovanelli (Cornell)
Project Manager: Thomas Sebring (Cornell)
Deputy Project Manager: Simon Radford (Caltech)
Project Scientists: Terry Herter (Cornell), Jonas Zmuidzinas (Caltech)

The survey described here is the work of the Cosmology science working group (S4), consisting of:

S. Golwala (Caltech) – Chair, R. Bean (Cornell), A. Blain (Caltech), J. Bock (JPL), A. Cooray (Caltech, U. California, Irvine), M. Dragovan (JPL), T. Gaier (JPL), J. Glenn (U. Colorado), E. Komatsu (U. Texas), A. Lange (Caltech), S. Myers (NRAO), A. Readhead (Caltech), S. Torchinsky (Cornell)

Baseline Survey

We propose five specific programs of different kinds and covering different mass ranges. S/N levels are per angular-resolution element and are valid out to the cluster virial radius.

High-Mass Cluster Mapping: 50 clusters with $M > 3.5 \times 10^{15}$ $M_\odot$ mapped to $S/N \geq 5$ (2 μK_{CMB})
Medium-Mass Cluster Mapping: 15 clusters with 1×10^{15} $M_\odot < M < 3.5 \times 10^{15}$ $M_\odot$ mapped to $S/N \geq 3$ (1 μK_{CMB})
Medium-Mass Cluster Radial Profiling: 1000 clusters with 1×10^{15} $M_\odot < M < 3.5 \times 10^{15}$ $M_\odot$ mapped to $S/N \geq 0.3$ (10 μK_{CMB}), which provides azimuthally averaged radial profiles with $S/N \gtrsim 5$
Low-Mass Cluster Radial Profiling: 100 clusters with 3.5×10^{14} $M_\odot < M < 1 \times 10^{15}$ $M_\odot$ mapped to $S/N = 0.3$ (3 μK_{CMB}), providing radial profiles with $S/N \gtrsim 5$
Very Low-Mass Blind Survey: Survey of five 10 deg^2 fields to a mass limit of 1×10^{14} $M_\odot$

Blind tSZ surveys will in general reach a mass limit of approximately 3.5×10^{14} $M_\odot$. Therefore, the first four programs will provide data to test relations between tSZ flux and cluster mass in these surveys, while the final program will provide a means to measure empirically the wide-area surveys' detection efficiency functions at their mass threshold.

1 Scientific Motivation

1.1 The Sunyaev-Zeldovich Effects

The Sunyaev-Zeldovich effects consist of scattering of cosmic microwave background (CMB) photons by the hot electrons in the intracluster medium (ICM) of galaxy clusters. The thermal SZ (tSZ) effect is a spectral distortion of the CMB due to the shift in photon energy by Compton scattering [1]. The relation between cluster Comptonization parameter y and surface brightness and CMB temperature fluctuations is:

$$\frac{\Delta B_\nu}{B_\nu} = h(x)\,\frac{\Delta T_{\rm CMB}}{T_{\rm CMB}} = h(x)\,f(x)\,y \qquad y = \int n_e\,\frac{k\,T_e}{m_e\,c^2}\,\sigma_T\,dl \tag{1}$$

with

$$B_\nu(x) = 2\,k\,T_{\rm CMB}\left(\frac{\nu}{c}\right)^2\frac{x}{e^x-1} \qquad h(x) = \frac{x\,e^x}{e^x-1} \qquad f(x) = x\frac{e^x+1}{e^x-1} - 4 \tag{2}$$

where $x = h\,\nu/k\,T_{\rm CMB}$ is set by the observing frequency and y is the Comptonization parameter of the scattering medium. k is Boltzmann's constant, m_e, n_e, and T_e are the electron mass, density, and temperature, σ_T is the Thomson scattering cross section, and the integral is along the line of sight.

The tSZ effect has been detected in tens of clusters; John Carlstrom's group at University of Chicago dominates the count, having used the BIMA and OVRO interferometers to image about 60 clusters at 30 GHz [2]. The SuZIE experiment has the largest millimeter-wave sample, with a total of 11 clusters with measurements at 150, 220, and 275 or 350 GHz [3, 4]. No clusters have been found "blindly" in the tSZ yet. A significant deficiency of the existing data is their relatively poor angular resolution (about 1 arcmin) and their lack of ability to probe extended structure (because the sample is dominated by interferometric measurements).

The kinetic SZ (kSZ) effect is a Doppler shift of the CMB due to scattering by a moving cluster [5]. Since the focus of this document is tSZ mapping, kSZ studies will be neglected.

Frequency spectra of the tSZ and kSZ effects, and of the CMB, are shown in Figure 1.

1.2 Cluster Astrophysics using the tSZ Effect

There is a very compelling case to be made for the study of galaxy clusters using tSZ. The tSZ effect essentially measures the line-of-sight integral of the gas pressure in a cluster. This is an observable that is central to any understanding of gas dynamics in the intracluster medium. Historically, free-free X-ray emission is our primary probe of intracluster gas. X-ray emission is a complicated observable: it measures the product of the square of the electron density, n_e^2, and the nontrivial electron-temperature dependent emissivity function, $\Lambda(E_X, T_e)$. While Chandra and XMM have taught us a great deal, they have also more than adequately proven how complicated the ICM is, with cold fronts, bubbles from AGN, evidence of mergers, etc. tSZ would provide us with another ICM observable, one that is more simply related to a physical quantity (the pressure) than X-ray emission. tSZ profiles of clusters would allow more detailed study of the thermodynamic state of the gas, including the level of entropy injection by star formation or other heating processes, the importance of radiative cooling, and cluster merger histories. tSZ may also give us more information about the shape of the gravitational potential well – the dark matter – and the gas profile, as tSZ will naturally extend out to larger radius than X-ray emission.

1.3 Blind tSZ Surveys and Supplementary High Angular Resolution Observations

An exciting prospect for SZ work in the coming years is the advent of large-area "blind" surveys in the tSZ. The tSZ provides a largely redshift-independent method for detecting galaxy clusters; a

flux-limited tSZ survey is, to a factor of 2, a mass-limited survey [6]. Thus, measurement of cluster abundance as a function of redshift via the tSZ would be free of the extremely redshift-dependent selection function one finds for optical or X-ray surveys for clusters. Such a cluster abundance measurement would constrain cosmological parameters, in particular Ω_m, Ω_Λ, and the equation of state parameter w [7]. A number of such surveys will be undertaken in the coming years by the Atacama Pathfinder Experiment-SZ (APEX-SZ – MPIfR and Berkeley), the Atacama Cosmology Telescope (ACT – Princeton, Penn, Goddard), the South Pole Telescope (SPT – Chicago, Case Western, and Berkeley), and the Planck satellite. They will cover hundreds to thousands of square degrees and detect thousands of clusters.

The ability of such surveys to derive cosmological implications will depend sensitively on their ability to relate observed tSZ fluxes to cluster masses. To optimize detection rates, the surveys do not resolve their target clusters, and thus obtain no information on departures from ideal cluster models. They will rely on scaling relations [7, 8, 9], follow-up data [10, 11], and self-calibration [12, 13] to obtain mass estimates. Prospects for these methods are quite good. Nevertheless, a high-angular resolution study of a subset of the clusters detected in these surveys would provide the ideal way to perform tests and cross-checks of these techniques.

The mass limit of a wide-area survey is set essentially by its angular resolution. Clusters that are significantly smaller than the survey angular resolution are not efficiently detected due to beam dilution. Infrared and radio point sources present a "confusion limit", a flux below which the density of point sources is so high that the survey noise becomes limited by pixel-to-pixel fluctuations in the number of such sources rather than by instrument sensitivity. Thus, a survey with better angular resolution than the 1- to 1.5-arcmin FWHM surveys planned for APEX-SZ, ACT, and SPT will reach a lower mass limit. Such a survey on a set of small fields would provide a means to test the wide-area surveys' detection efficiency functions.

2 The Cornell-Caltech Atacama Telescope and tSZ Applications

In late 2003, a group from Cornell, Caltech, and JPL came together to study the possible uses of a 25-m telescope with high surface accuracy in submillimeter bands and operating at a high, dry site. Such a facility would provide significant improvement over the SCUBA and IRAM telescopes, which have angular resolutions of 15 arcsec and 10 arcsec (at the maximum survey frequencies allowed by their sites, 350 GHz and 250 GHz, respectively). The new facility's primary desired features were found to be: 1) location at a high, dry site that would provide significant amounts of time with good atmospheric transmission at 850 GHz; 2) a very precise surface (12 μm rms) to enable high aperture efficiency at 850 GHz; 3) a large aperture to provide high angular resolution, thereby reducing the limitiations imposed by confusion noise; and 4) a wide field-of-view (> 5 arcmin) to enable fast surveying. Such a telescope would provide an unprecedented ability to perform surveys for extragalactic dusty sources.

There was great enthusiasm for this venture, dubbed the Cornell-Caltech Atacama Telescope (CCAT), to be sited in the Atacama Desert in Chile near the ALMA site. A \$1M feasibility study is ongoing, with a final report expected in January, 2006. Assuming funding is available as planned, CCAT will expect to see first light in 2012.

A variety of other exciting science would be enabled by such a telescope. The focus of this document is the use of the telescope to map galaxy clusters in the tSZ effect at 150 GHz with sufficient angular resolution to resolve the clusters. The excellent site ensures that tSZ observations at 150 GHz would be possible most of the time; for reference, the atmospheric opacity at this frequency is less than 0.05 for about 60% of the year (including daytime hours) [14]. The large aperture provides the desired angular resolution, sufficient to resolve galaxy clusters but coarse enough that the field-of-view can encompass an entire cluster and that the focal plane detector

pixel count is reasonable.

Due to the fact that CCAT is still in the very early study stage, detailed quantitative estimates of scientific return of various kinds of tSZ studies are not yet available. This document is instead framed as a semi-quantitative summary of signal sizes and expected signal-to-noise achievable on cluster tSZ imaging and radial profiles. We show that such tSZ work is feasible and, at the depth studied so far, scientifically interesting.

3 Sunyaev-Zeldovich Observables

There is a large literature on calculating the expected dark-matter and gas profiles of galaxy clusters, the resulting tSZ profiles, and the abundances of clusters (*e.g.*, [15, 16, 17, 18, 19, 20, 6, 21, 22, 23, 24, 25, 26, 20, 27, 28, 29, 30, 31, 32]). We have reviewed this literature and calculated simple approximate formulae for basic quantities of interest. Based on these, we present numerical estimates of various tSZ observables – cluster abundances, cluster sizes, and signal levels.

3.1 Assumptions

The fiducial cluster we would like to detect is one at the mass limit of the wide-area tSZ surveys such as APEX-SZ, ACT, and SPT, with $M \approx 3.5 \times 10^{14}$ $M_\odot$ [22]. Other fiducial targets would be clusters with masses of 10^{14} $M_\odot$, 10^{15} $M_\odot$, and 3.5×10^{15} $M_\odot$. The Planck all-sky survey is expected to detect clusters down to a mass limit of 8×10^{14} $M_\odot$ [22].

For reference, we will assume a Gaussian illumination of a 25-m diameter primary with a conservative -10 dB edge taper. The illumination pattern has $\sigma = 5.8$ m and FWHM = 13.7 m. At 150 GHz, the angular resolution (FWHM) will be 0.44 arcmin = 26 arcsec.

3.2 Numerical Estimates of Abundances, Angular Scales, and Signal Levels

In Table 1, we list some numerical estimates of cluster abundances, angular scales, and signal levels. These estimates are a mix of simple analytic calculations (NFW dark matter profile [15] + β-model gas profile [20]) and simulations (used for normalization purposes, primarily [30]). All cluster parameters are dependent on the redshift of cluster formation (z_f) and of observation (z_o). We take values of these that yield the most conservative values of the observables. Signal levels in μK_{CMB} are computed at 150 GHz.

Some important notes regarding the table:

- If a single range of values is listed for the full set of masses, than the dependence on z_f and z_o is stronger than on mass.
- Neither the scale radius nor the virial radius provide a true characteristic extent of the SZ signal, being either too small or too large. The geometrical mean of the two, $r_g = \sqrt{R_v\, r_c}$, is more appropriate.
- The β-profile core radii from theory tend to underpredict the data in massive clusters like CL0016+16; we have artificially extended the upper end of the range by a factor of 2 to accomodate the data.
- In converting from radii to angle, the conversion factor is 2.5 for $z > 1$, increasing to 5 at $z = 0.25$. We have applied 2.5 to the smallest clusters and 5 to the largest clusters to indicate the possible range.
- For tSZ signals, the numbers are underestimates in that the we have taken z_f so as to minimize the signal, but are overestimates for signals at r_c and r_g since these depend on the halo and gas concentrations, which we may have overpredicted. The virial signal values are always underestimates because they do not depend on the concentration parameters.

4 Expected Instrumentation and Sensitivity

4.1 Choice of Frequency Band

The nominal frequency band of choice for tSZ observations with CCAT will be 150 GHz for a number of reasons. Higher frequencies (300 GHz to 400 GHz) provide larger surface brightness fluctuations, but atmospheric fluctuation noise and confusion noise from infrared point sources are significantly worse [33]. At frequencies below the 85 GHz to 105 GHz atmospheric window, CCAT provides no significant gains over existing or planned instrumentation in terms of angular resolution. The 100 GHz window would be a reasonable choice, but the SZA, already in operation at 30 GHz, will have access to that band at a much earlier date; also, there is a moderate loss of angular resolution as compared to 150 GHz.

4.2 Sensitivity

With conservative assumptions of 10% telescope emissivity and operation in $\tau = 0.05$ atmospheric opacity conditions, the background-limited instantaneous sensitivity of a 150 GHz camera on CCAT would be 2.3 mJy $\mathrm{s}^{1/2}$ (310 $\mu\mathrm{K}_{\mathrm{CMB}}$ $\mathrm{s}^{1/2}$). CCAT's optical design provides a 20 arcmin field-of-view, large enough to fully contain the virial extent of almost any galaxy cluster at $z \gtrsim 0.25$. This field-of-view can be filled with 500 pixels of size $2\,(F/\#)\,\lambda$.

4.3 Availability of Detector Technology

Existing bolometric detectors are able to provide this background-limited sensitivity using feedhorn-coupled spiderweb absorbers and semiconducting thermistors [34, 35]. Such "spiderweb bolometers" have been used or are in use a large number of suborbital experiments – BOOMERANG, MAXIMA, ARCHEOPS, ACBAR, QUAD, and BICEP – and will be flown on both the Herschel and Planck satellites. A pixel count almost as large as CCAT requires has been demonstrated in the field with bare-absorber bolometers in the SHARC-II camera on the Caltech Submillimeter Observatory (384 pixels). A significantly larger array of bare-absorber bolometers (thousands of pixels) will be deployed for the SCUBA-2 camera on the James Clerk Maxwell Telescope. (Both SHARC-II and SCUBA-2 detectors would not meet the sensitivity needs of a CCAT 150 GHz camera.)

One excellent candidate technology that would provide both the necessary instantaneous sensitivity as well as the high pixel count is antenna-coupled detectors [36, 37, 38, 39]. Such detectors receive optical power with a phased array of superconducting slot dipole antennae and couple this optical power to a bolometric detector via superconducting microstrip. All elements are fabricated by photolithography on a single silicon wafer. The phased-array approach has a very controlled radiation pattern, minimizing susceptibility to stray light and ensuring that the detectors will be limited by optical loading from the telescope and sky rather than from stray light inside the camera. Yet phased arrays, being entirely photolithographic, are almost CCD-like in their simplicity, which ensures that fabrication of such a large array is feasible and minimizes the focal plane mass (which must be cooled to 300 mK for bolometric detectors) by obviating feedhorns.

Antenna-coupled detectors are currently under development at JPL and Caltech by a group led by J. Bock and J. Zmuidzinas using both superconducting transition-edge sensors (TESs) [40, 41] and microwave kinetic inductance detectors (MKIDs) [42, 43] as the bolometric sensors. Single pixels of both kinds have now been demonstrated; a demonstration of a 64-pixel array is expected soon.

There exist multiplexed electronic readout systems for both TESs and MKIDs, so readout of a 500-pixel array should not prove a technical challenge. In fact, the TES multiplexing system that would likely be used, developed by a group at NIST [44, 45, 46, 47], will be used for SCUBA-2 and so will have an excellent in-the-field demonstration by the time it might be needed for CCAT. MKID

multiplexing has also been demonstrated for arrays of 50 sensors, with no significant technical obstacles preventing a scale-up to 500 pixels [48].

4.4 Budgetary Considerations

Rough estimates based on the personnel requirements and historical cost of similar instrumentation suggest that such a camera will cost in the vicinity of \$5M to build. The bulk of the cost is in salary support; \$1M per year over a 5-year build would support a fabrication technician, 2 engineers, 2 postdocs, and 2-3 graduate students. Given the scale of the telescope (\$50M to \$100M) and the already-funded wide-area tSZ survey instrumentation (likely $\geq$ \$10M for ACT and $\geq$ \$30M for SPT), this construction cost for such an important follow-up instrument does not seem unreasonable.

5 Scientific Reach

5.1 Naive Integration Times

In Table 2, we list integration times for the various science targets listed in Table 1 using a sensitivity of 310 $\mu\mathrm{K_{CMB}}$ $\mathrm{s}^{1/2}$. We assume atmospheric emission fluctuations (sky noise) are sufficiently common-mode to be perfectly removed by a single array-average sky template, that the cluster or science target is always on the array, and we neglect confusion for this simple calculation. We calculate the time needed to reach $S/N = 5$ in each beam, so that one is truly obtaining a map.

We defer discussion of specific science projects until after confusion has been discussed.

5.2 Confusion Limits

The dominant source of confusion at SZ frequencies is extragalactic infrared point sources. We present confusion limits from A. Blain [33]. The *1 source per beam* confusion limits are given in Table 3. The confusion limit at 150 GHz is higher than the tSZ signal level in the wings of $3.5 \times 10^{14}\,\mathrm{M_\odot}$ and 1×10^{15} $\mathrm{M_\odot}$ clusters and is comparable to the tSZ signal level at r_g in $3.5 \times 10^{14}\,\mathrm{M_\odot}$ clusters. Confusion is clearly a challenge.

It is expected confusion noise may be subtracted using maps made at higher frequencies. The limit on how well this can be done is set by the confusion limit in the higher-frequency bands – assuming one knows the source spectral index perfectly, the systematic error on removing a source based on its high-frequency flux is set by the uncertainty on that high-frequency flux, which can be no smaller than the confusion noise.

Confusion noise is not Gaussian and depends on the source count power-law slope of the confusing source distribution. Nevertheless, it is conventional to require no more than 1 source every 30 beams when considering 5σ point-source detections and no more than 1 source every 10 beams when considering 3σ point-source detections. So, useful figures of merit are obtained by scaling the 350 GHz and 490 GHz 1-source-per-30-beams and 1-source-per-10-beams fluxes to the SZ bands using a standard $\nu^{1.7}$ emissivity law: to first order, we will assume that the 1-source-per-30-beams and 1-source-per-10-beams levels provide the signal levels at which one can obtain no better than $S/N = 5$ and $S/N = 3$ per beam, respectively, in the SZ map.[1] These scaled fluxes are listed in Table 4, which indicate that it is possible to remove sources to well below the 150 GHz 1-source-per-beam confusion limit. Further statistical suppression of confused sources might be obtained by using confused high-frequency maps in some sort of joint multifrequency map estimation.

ALMA follow-up to identify and measure the fluxes of confusing point sources in-band is an obvious prospect to consider, but the field-of-view of ALMA is so small that one can only cover small regions to sufficient depth in a reasonable time.

[1] Reaching the confusion limit on one field-of-view at 350 GHz and 490 GHz with CCAT only requires 1200 sec and 4500 sec, so it is expected that all SZ fields can be covered to the high-frequency confusion limit.

5.3 Candidate SZ Key Projects

Given the above tables of signal levels, integration times, and confusion limits, and the aforementioned 310 μK_{CMB} $s^{1/2}$ instantaneous sensitivity, we have calculated in Table 5 the cluster samples obtained in and total survey times needed for a set of five tSZ key projects. They are briefly summarized in the list below. We have aimed for a number of programs that each require no more than 100 to 200 hours per year and are conducted over 5-year periods. Based on the observed atmospheric opacity distributions, it would be reasonable for all 5 projects to occur simultaneously. S/N levels are per angular-resolution element and are valid out to the cluster virial radius.

High-Mass Cluster Mapping: 50 clusters with $M > 3.5 \times 10^{15}$ $M_\odot$ mapped to $S/N \geq 5$ (2 μK_{CMB})

Medium-Mass Cluster Mapping: 15 clusters with 1×10^{15} $M_\odot < M < 3.5 \times 10^{15}$ $M_\odot$ mapped to $S/N \geq 3$ (1 μK_{CMB})

Medium-Mass Cluster Radial Profiling: 1000 clusters with 1×10^{15} $M_\odot < M < 3.5 \times 10^{15}$ $M_\odot$ mapped to $S/N \geq 0.3$ (10 μK_{CMB}), which provides azimuthally averaged radial profiles with $S/N \gtrsim 5$

Low-Mass Cluster Radial Profiling: 100 clusters with 3.5×10^{14} $M_\odot < M < 1 \times 10^{15}$ $M_\odot$ mapped to $S/N = 0.3$ (3 μK_{CMB}), providing radial profiles with $S/N \gtrsim 5$

Very Low-Mass Blind Survey: Survey of five 10 deg^2 fields to a mass limit of 1×10^{14} $M_\odot$

Blind tSZ surveys will in general reach a mass limit of approximately 3.5×10^{14} $M_\odot$. Therefore, the first four programs will provide data to test relations between tSZ flux and cluster mass in these surveys, while the final program will provide a means to measure empirically the wide-area surveys' detection efficiency function at their mass threshold.

In addition to full mapping applications, we have presented two tSZ "radial profile" key projects, in which azimuthal averaging will be used to obtain tSZ radial profiles for large catalogs of sources in reasonable amounts of telescope time. Of course, detailed information about azimuthal variations is lost. Expected profiles with uncertainties are shown in Figure 2. The choice of sensitivities for these projects was made so as to achieve $S/N \approx 5$ in each radial bin at large radius. This sensitivity easily allows one to distinguish the three different β-profile exponents $\beta = 0.6$, 0.67, and 0.75. The per-beam sensitivity needed to obtain these radial profiles is a factor of 10 poorer than what is needed for full mapping, enabling the study of 100 times as many clusters.

Quantitative evaluation of the scientific merit of these projects awaits detailed simulation work, which will be undertaken during the ongoing CCAT study. But, clearly, the signal-to-noise levels achieved are sufficient for true mapping of high- and medium-mass clusters, and will provide quite precise azimuthally averaged radial profiles of very large catalogs of clusters. Without a doubt, such information will be of great use to the wide-area tSZ surveys.

6 Uniqueness and Complementarity

The case has already been made for the complementarity of CCAT tSZ work to the wide-area surveys by APEX-SZ, ACT, SPT, and Planck. In the wider field of SZ instrumentation, current and upcoming, CCAT will also have a unique and complementary role to play:

- The Sunyaev-Zeldovich Array (SZA) is an interferometer designed for blind tSZ surveying at 30 GHz. It is sited at CARMA and is currently taking survey data. It will begin to study cluster substructure at 90 GHz. The SZA, being an interferometer, will have a better understanding of systematic effects of observing technique but will have significantly poorer instantaneous sensitivity due to its factor of 6-7 smaller collecting area, poorer site, and use

of heterodyne receivers. Together, SZA and CCAT will provide SZ spectral coverage at high angular resolution from 30 GHz to 150 GHz.

A possible eventual upgrade of SZA for higher frequency operation is not likely to pose much competition to CCAT given the latter's better site and more sensitive receivers.

- The Penn Array is a 64-pixel 90 GHz bolometric array being built for the Green Bank Telescope (GBT). The instrument will have angular resolution 8 arcsec (0.13 arcmin) and 0.5 arcmin field-of-view, which enables it to investigate SZ substructure on few arcsec scales, but it will lose sensitivity on arcminute scales due to sky noise; it thus complements CCAT.

- The Large Millimeter Telescope (LMT) will provide information on scales comparable to GBT or midway between CCAT and GBT. The LMT design provides a 4 arcmin field-of-view, and currently planned instrumentation (AzTEC) will cover a 1.5 arcmin field-of-view. The LMT angular resolution at 150 GHz is comparable to that of GBT at 90 GHz. Atmospheric conditions might favor 90 GHz operation instead, in which case LMT provides angular resolution midway between that of CCAT and GBT. The better angular resolution of the LMT in the 150-300 GHz range as compared to CCAT is cancelled by CCAT's ability to observe in the 350 GHz and 490 GHz bands, which are inaccessible to LMT.

- Interferometers like CARMA and ALMA will have exquisite sensitivity over a field-of-view of a fraction of an arcmin^2 at the frequencies of interest for SZ. They will provide high angular resolution probes of substructure in the SZ, but will have poor fidelity on scales much larger than 1 arcmin, as well as being too slow to map fields appreciably larger than 10 arcmin^2.

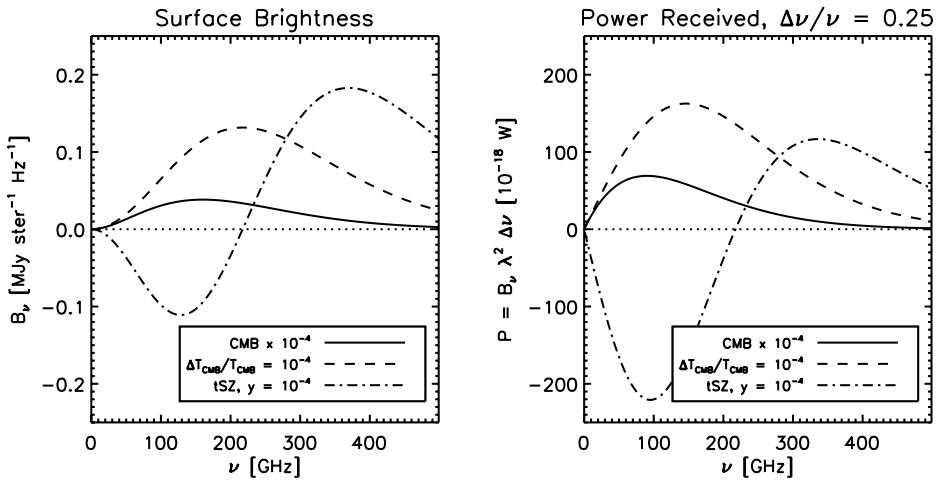

Figure 1: CMB and SZ frequency spectra. Solid curve: CMB. Dashed curve: CMB temperature anistropy at $\Delta T_{\rm CMB}/T_{\rm CMB} = 10^{-4}$ (comparable to primary anisotropy on 1 degree angular scales). Dash-dot curve: thermal SZ (tSZ) effect for $y = 10^{-4}$ ($\tau = 0.005$ and $T_e \sim 10$ keV $\approx 0.02\, m_e\, c^2$), typical of a massive, nearby cluster. The dashed curve also holds for kinetic SZ (kSZ) with $(v/c)\,\tau = 10^{-4}$ (a massive cluster with $\tau = 0.005$ and $v = 600$ km/s, larger than expected by a factor of a few). Right: power incident on a receiver assuming 25% fractional bandwidth and single-optical-mode design.

Parameter	Cluster Mass [$M_\odot$] 1×10^{14}	3.5×10^{14}	1×10^{15}	3.5×10^{15}
Abundance > M [deg^{-2}]	40	6	0.25	0.012
Number in 20000 deg^2 > M	10^6	10^5	few $\times 10^3$	10^2
virial radius R_v [Mpc]	1 – 5			
β-profile core radius r_c [Mpc]	0.05 - 0.3			
$r_g = \sqrt{R_v\, r_s}$ [Mpc]	0.2 – 1.2			
virial angle θ_v [arcmin]	2.5 – 25			
core radius θ_c [arcmin]	0.1 – 0.6			
$\theta_g = \sqrt{\theta_v\, \theta_s}$ [arcmin]	0.5 – 4			
optical depth for Thomson scattering				
central, τ_0	10^{-3} – 10^{-2}			
at r_g, τ_g	10^{-4} – 10^{-3}			
Comptonization parameter, y				
at r_c	2×10^{-6}	7×10^{-6}	2.5×10^{-5}	1×10^{-4}
at r_g	4×10^{-7}	2×10^{-6}	6×10^{-6}	2.5×10^{-5}
at R_v	$> 7 \times 10^{-8}$	$> 3 \times 10^{-7}$	$> 1 \times 10^{-6}$	$> 4.5 \times 10^{-6}$
tSZ $\Delta T_{\rm CMB}$ at 150 GHz [μK$_{\rm CMB}$]				
at r_c	5	20	65	300
at r_g	1	5	15	70
at R_v	> 0.2	> 1	> 3	> 10
tSZ flux/beam at 150 GHz [μJy]				
at r_c	30	140	450	2000
at r_g	8	35	100	500
at R_v	> 1.4	> 6	> 20	> 90
tSZ total flux at 150 GHz [mJy]	> 0.35	> 3.5	> 24	> 230
	> 50 μJy at 3.5×10^{13} $M_\odot$			

Table 1: Numerical estimates. See text for notes.

target	signal level μK$_{\rm CMB}$	μJy	time [ksec]	time [hours at 50% obs. eff.]
tSZ profiles, $S/N = 5$ per beam				
at r_g, M = 3.5×10^{15} $M_\odot$	70	500	0.5	0.3
virial wings, M = 3.5×10^{15} $M_\odot$	10	75	24	13
at r_g, M = 1×10^{15} $M_\odot$	15	100	11	6
virial wings, M = 1×10^{15} $M_\odot$	3	23	270	150
at r_g, M = 3.5×10^{14} $M_\odot$	5	35	100	55
virial wings, M = 3.5×10^{14} $M_\odot$	1	7.5	2400	1300
tSZ pt-src survey, $S/N = 5$ at mass limit				
10 deg^2 to 1×10^{14} $M_\odot$	50	350	85	50
0.5 deg^2 to 3.5×10^{13} $M_\odot$	7	50	220	120

Table 2: Expected integration times to obtain $S/N = 5$ per beam for various science targets, all at 150 GHz.

frequency	flux density	temperature	y parameter
275 GHz	66 μJy	27 μK_{CMB}	1.1×10^{-5}
220 GHz	89 μJy	21 μK_{CMB}	N/A
150 GHz	44 μJy	6 μK_{CMB}	2.3×10^{-6}
100 GHz	21 μJy	2.1 μK_{CMB}	5.1×10^{-7}

Table 3: One-source-per-beam confusion limits

	350 GHz		490 GHz	
frequency	1 src per 30 beams [μJy]	1 src per 10 beams [μJy]	1 src per 30 beams [μJy]	1 src per 10 beams [μJy]
in-band	830	390	1200	500
275 GHz	340	160	140	59
220 GHz	150	70	62	26
150 GHz	36	17	15	6.3
100 GHz	8.1	3.8	3.4	1.4

Table 4: Confusion levels in high-frequency bands scaled to SZ bands.

	per beam sensitivity			# of objects per	# of hours per	# of objects in 5	# of hours in 5	confusion (# srces per 490 GHz
Science target	μK_{CMB}	μJy	S/N	year	year	years	years	beam)
tSZ profiles								
High-mass ($> 3.5 \times 10^{15}$ $M_\odot$)								
mapping	2	15	5	10	130	50	650	1 per 30
Medium-mass (1×10^{15} $M_\odot$ – 3.5×10^{15} $M_\odot$)								
mapping	1	7.5	3	3	160	15	800	$\sim$ 1 per 10
radial profile	10	75	0.3	200	100	1000	600	$\ll$ 1 per 30
Low-mass (3.5×10^{14} $M_\odot$ – 1×10^{15} $M_\odot$)								
radial profile	3	23	0.3	20	120	100	600	$<$ 1 per 30
tSZ pt-src survey, $S/N = 5$ at 1×10^{14} $M_\odot$ on 10 deg^2 fields								
	10	75	5	1	50	5	150	$\ll$ 1 per 30

Table 5: Candidate SZ key projects. The "confusion" column refers to the number of sources per 490 GHz beam at the flux level obtained by scaling the low-frequency per-beam sensitivity to 490 GHz using $\nu^{3.7}$.

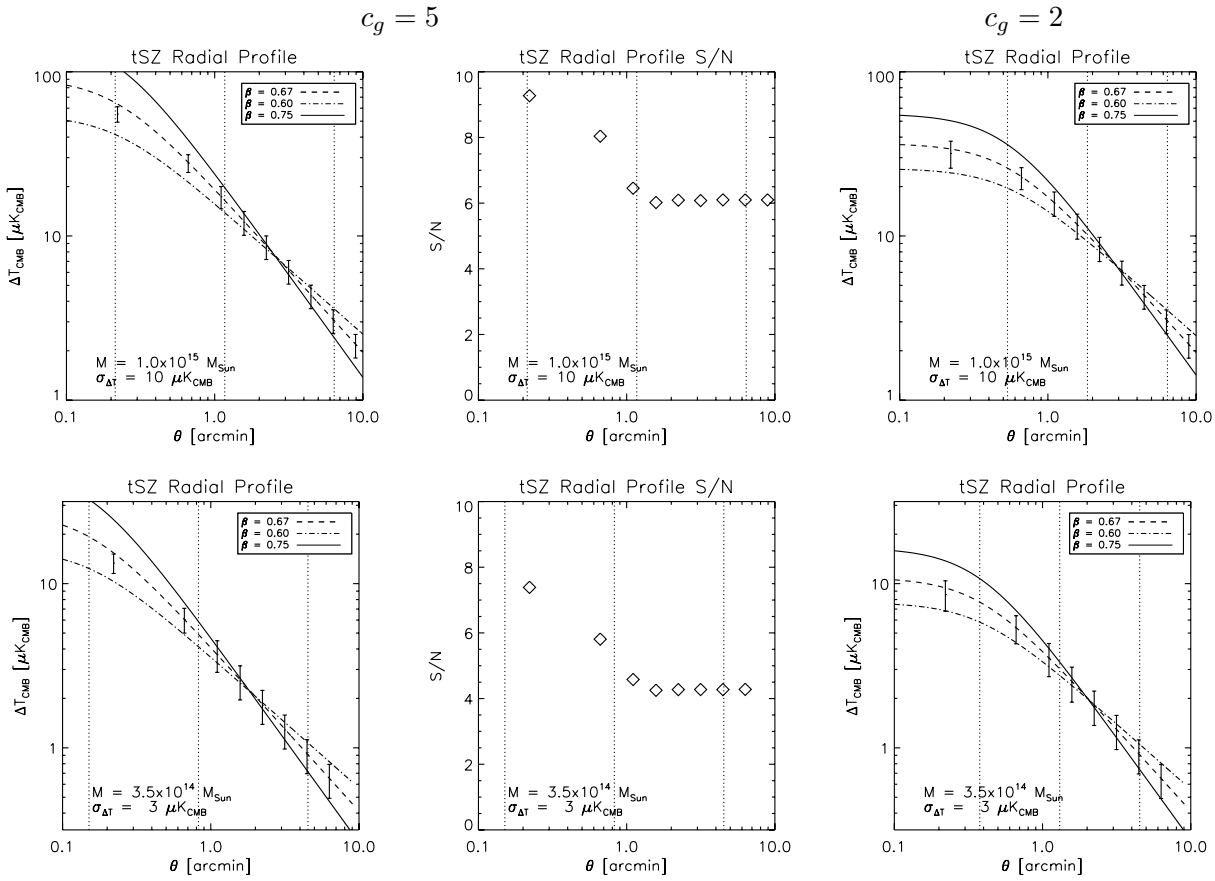

Figure 2: Expected errors on tSZ radial profiles. Cluster masses and assumed per-beam sensitivies are indicated. Each plot also shows three different β profiles that would yield the same integrated SZ Comptonization parameter within R_v. Profiles for two different values of the gas concentration factor, c_g, are shown; c_g is the ratio of the dark-matter halo NFW scale radius to the the gas β-profile core radius. The vertical dotted lines indicate the three radii r_c, r_g, and R_v. The radial binning of the data is linear at small radius and logarithmic at large radius; no bin is allowed to be smaller than the beam FWHM at 150 GHz. The increase with radius of the area per bin yields approximate constant $S/N \approx 5$ at large radius.

References

[1] R. A. Sunyaev and Y. B. Zeldovich, Comm. Astr. Sp. Phys. **4**, 173 (1972).

[2] J. E. Carlstrom, G. P. Holder, and E. D. Reese, Annu. Rev. Astro. Astroph. **40**, 643 (2002).

[3] B. A. Benson *et al.*, Astroph. J. **592**, 674 (2003).

[4] B. A. Benson *et al.*, Astroph. J. **617**, 829 (2004).

[5] R. A. Sunyaev and I. B. Zeldovich, Mon. Not. Roy. Astron. Soc. **190**, 413 (1980).

[6] G. P. Holder *et al.*, Astroph. J. **544**, 629 (2000).

[7] Z. Haiman, J. J. Mohr, and G. P. Holder, Astroph. J. **553**, 545 (2001).

[8] J. Weller, R. A. Battye, and R. Kneissl, Phys. Rev. Lett. **88**, 231301 (2002).

[9] E. S. Levine, A. E. Schulz, and M. White, Astroph. J. **577**, 569 (2002).

[10] S. Majumdar and J. J. Mohr, Astroph. J. **585**, 603 (2003).

[11] S. Majumdar and J. J. Mohr, Astroph. J. **613**, 41 (2004).

[12] W. Hu, Phys. Rev. D **67**, 081304 (2003).

[13] M. Lima and W. Hu, Phys. Rev. D **70**, 043504 (2004).

[14] S. J. E. Radford, private communication.

[15] J. F. Navarro, C. S. Frenk, and S. D. M. White, Astroph. J. **490**, 493 (1997).

[16] M. Birkinshaw, Phys. Rep. **310**, 97 (1999).

[17] R. K. Sheth and G. Tormen, Mon. Not. Roy. Astron. Soc. **308**, 119 (1999).

[18] A. Jenkins *et al.*, Mon. Not. Roy. Astron. Soc. **321**, 372 (2001).

[19] U. Seljak, Mon. Not. Roy. Astron. Soc. **318**, 203 (2000).

[20] E. Komatsu and U. Seljak, Mon. Not. Roy. Astron. Soc. **327**, 1353 (2001).

[21] G. P. Holder and J. E. Carlstrom, Astroph. J. **558**, 515 (2001).

[22] G. Holder, Z. Haiman, and J. J. Mohr, Astroph. J. Lett. **560**, L111 (2001).

[23] J. S. Bullock *et al.*, Mon. Not. Roy. Astron. Soc. **321**, 559 (2001).

[24] N. Makino, S. Sasaki, and Y. Suto, Astroph. J. **497**, 555 (1998).

[25] A. R. Cooray, Ph.D. thesis, University of Chicago, 2001.

[26] Y. Suto, S. Sasaki, and N. Makino, Astroph. J. **509**, 544 (1998).

[27] A. J. Benson, C. Reichardt, and M. Kamionkowski, Mon. Not. Roy. Astron. Soc. **331**, 71 (2002).

[28] R. H. Wechsler *et al.*, Astroph. J. **568**, 52 (2002).

[29] D. H. Zhao, H. J. Mo, Y. P. Jing, and G. Börner, Mon. Not. Roy. Astron. Soc. **339**, 12 (2003).

[30] A. C. da Silva, S. T. Kay, A. R. Liddle, and P. A. Thomas, Mon. Not. Roy. Astron. Soc. **348**, 1401 (2004).

[31] I. G. McCarthy, A. Babul, G. P. Holder, and M. L. Balogh, Astroph. J. **591**, 515 (2003).

[32] P. M. Motl, E. J. Hallman, J. O. Burns, and M. L. Norman, astro-ph/0502226, submitted to Astroph. J. Lett.

[33] A. W. Blain, private communication.

[34] B. P. Crill *et al.*, Astroph. J. Suppl. **148**, 527 (2003).

[35] M. C. Runyan *et al.*, Astroph. J. Suppl. **149**, 265 (2003).

[36] A. Goldin *et al.*, AIP Conf. Proc. 605: Low Temperature Detectors **605**, 251 (2002).

[37] A. Goldin *et al.*, in *Proceedings of the SPIE, Vol. 4855: Millimeter and Submillimeter Detectors for Astronomy*, edited by T. G. Phillips and J. Zmuidzinas (SPIE, Bellingham, Washington, 2003), pp. 163–171.

[38] A. Goldin *et al.*, in preparation.

[39] A. Vayonakis *et al.*, AIP Conf. Proc. 605: Low Temperature Detectors **605**, 539 (2002).

[40] K. D. Irwin, Appl. Phys. Lett. **66**, 1998 (1995).

[41] C. L. Hunt *et al.*, in *Proceedings of the SPIE, Vol. 4855: Millimeter and Submillimeter Detectors for Astronomy*, edited by T. G. Phillips and J. Zmuidzinas (SPIE, Bellingham, Washington, 2003), pp. 318–321.

[42] P. K. Day *et al.*, Nature **425**, 817 (2003).

[43] B. A. Mazin *et al.*, in *Proceedings of the SPIE, Vol. 4849: Highly Innovative Space Telescope Concepts*, edited by H. A. MacEwen (SPIE, Bellingham, Washington, 2002), pp. 283–293.

[44] J. A. Chervenak *et al.*, Appl. Phys. Lett. **74**, 4043 (1999).

[45] P. A. J. de Korte *et al.*, Rev. Sci. Instr. **74**, 3807 (2003).

[46] C. D. Reintsema *et al.*, Rev. Sci. Instr. **74**, 4500 (2003).

[47] K. D. Irwin *et al.*, Nucl. Instrum. Meth. A **520**, 544 (2004).

[48] J. Zmuidzinas, private communication.